Solar Energy Materials & Solar Cells 157 (2016) 533–542

Contents lists available at ScienceDirect

Solar Energy Materials & Solar Cells

journal homepage: www.elsevier.com/locate/solmat

Experimental and numerical study of metal-oxides/water nanofluids as coolant in photovoltaic thermal systems (PVT)

Mohammad Sardarabadi, Mohammad Passandideh-Fard *

Department of Mechanical Engineering, Ferdowsi University of Mashhad, Mashhad, Iran

ARTICLE INFO

Article history:
Received 29 January 2016
Received in revised form
27 June 2016
Accepted 8 July 2016

Keywords:
Photovoltaic thermal system
Metal-oxides/water nanofluids
Numerical and experimental study

ABSTRACT

In this study, the use of metal-oxides/water nanofluids as coolants in photovoltaic thermal units (PVT) is investigated experimentally and numerically. The considered nanoparticles include Aluminum-oxide (Al_2O_3), Titanium-oxide (TiO_2) and Zinc-oxide (ZnO) all dispersed in deionized water as base fluid, with 0.2% by weight (wt%). To investigate the reliability of the measurements, an uncertainty analysis is performed for the experimental data. The *t-statistic* indicator is used to verify that the results of the numerical model are statistically significant. The electrical efficiency for the PVT system is calculated based on the measured temperature of the photovoltaic surface and the fluid outlet. The energy balance equations for various parts of the PVT system are solved using numerical simulations. Both numerical and experimental results show that the TiO_2/water and ZnO/water nanofluids present a better performance in terms of the electrical efficiency compared to that of the Al_2O_3/water nanofluid and deionized water. In terms of the thermal performance of the system, the ZnO/water nanofluid is found to have the highest thermal efficiency compared to deionized water and the other two nanofluids. Finally, the numerical model is used to investigate the effect of nanoparticles mass fraction, ranged from 0.05 to 10 wt%, on electrical and thermal performance of the PVT system.

1. Introduction

A photovoltaic thermal system (PVT) consists of a conventional photovoltaic unit (PV) which converts photons diffused from the sun into electricity, and a thermal collector which absorbs both the remaining energy of photons and the heat produced by the photovoltaic cells. A simultaneous generation of electricity and heat makes these systems more efficient compared to conventional PV units or solar thermal collectors. In recent years, there has been an increased interest in exploring new techniques to improve the efficiency of these systems. Many numerical/experimental attempts have been performed for this purpose by varying the collector structure [1–4]; the type of photovoltaic cells [5]; employing concentration systems [6]; and applying various working fluid such as air, water, and nanofluids [7–9]. Although the structural design is an important factor to have an efficient system, the design variations in a PVT system are very limited. As an example, the thermal efficiency of a sheet-and-tube collector is only 2% lower than that of other types of collectors (such as, channel, free flow and dual-absorber) [10]. Cerón et al. [11] used a 3D numerical model for tube-on-sheet flat-plate solar liquid collectors. Zhang et al. [12] studied the performance of a novel solar photovoltaic/loop-heat-pipe heat pump system. In their study, a dedicated computer model was developed to predict the system performance based on the heat balance principle. Their analysis showed that the exergetic efficiency of the thermal and electrical outputs of the system can reach 5.8% and 9.12%, respectively. In other words, the overall exergetic efficiency of the system can be as high as 14.92%.

Using a working fluid with enhanced heat transfer characteristics, such as nanofluids, can significantly improve the overall system efficiency without changing the structure design [7]. Several mechanisms reported in the literature for improving the heat transfer in nanofluids are: higher conductive heat transfer coefficient of nanoparticles [13], the Brownian motion of the nanoparticles [14], transient local heat transfer effects [15], and the electric charge on the surface of the nanoparticles [16]. Although the pressure drop due to nanoparticles is increased, this drawback is negligible in comparison with their heat transfer enhancement advantages [17]. A complete review of the use of nanofluids in solar collector applications can be seen in the work of Nagarajan et al. [18]. The main drawback of using nanofluids in the PVT systems originates from the fact that preparing a proper nanofluid suspension with a long-time stability is hard to achieve and can be quite costly. Therefore, in designing the PVT systems with nanofluids, performing numerical simulations may significantly reduce

* Corresponding author.
E-mail address: mpfard@um.ac.ir (M. Passandideh-Fard).

http://dx.doi.org/10.1016/j.solmat.2016.07.008
0927-0248/

Nomenclature

Parameters

A	surface area (m^2)
C	specific heat ($J\,kg^{-1}\,K^{-1}$)
G	solar irradiation ($W\,m^{-2}$)
h	heat transfer coefficient ($W\,m^{-2}\,K^{-1}$)
k	thermal conductivity ($W\,m^{-1}\,K^{-1}$)
Nu	Nusselt number
P	perimeter (m)
PF	packing factor
Pr	Prandtl number
PV	photovoltaic unit
PVT	photovoltaic thermal system
T	temperature
wt	weight

Subscripts

abs	absorber plate
amb	ambient
bf	base fluid
cond	conduction
cond	conduction
elec	electrical
env	environment
g	glass cover
ins	insulation
in	inlet
np	nanoparticle
oc	open circuit
out	outlet
sc	short circuit
tube	tube
th	thermal
w	wind

Greeks

α	absorption
β	solar cell temperature coefficient (K^{-1})
δ	thickness (m)
ρ	density ($kg\,m^{-3}$)
η	efficiency
τ	transmittance
ϕ	nanoparticles mass fraction in the base fluid
ε	emissivity

the number of required experiments. An overview of the reported literature on the PVT systems, show that combined numerical and experimental research especially for nanofluid-based-collectors is rare. Suganthi et al. [19] performed experiments on the ZnO/ethylene-glycol and ZnO/ethylene-glycol/water nanofluids as coolant fluids in presence of a constant heat flux boundary. They attributed the heat transfer enhancement to the increase of the thermal conductivity of the nanofluid. Bhattarai et al. [20] studied the transient process of a PVT system equipped with a sheet-and-tube water based collector using both experiments and simulations with a 1D mathematical model. He et al. [21] presented a theoretical and experimental study of a PVT system in a thermoelectric cooling and heating unit. They reported a high value of 16.7% and 23.5% for the electrical and thermal efficiencies of the PVT, respectively. The solar irradiation in their experiments changed from 200 to 700 W/m^2. A 2D thermal network model was introduced by Dehra [22] for a PV unit to predict the temperature distribution of a solar wall and the ventilation air requirements for ducts used in a photovoltaic hybrid system. Xu and Kleinstreuer [7] developed a 2D model coupling thermal analysis and CFD simulations to calculate efficiencies of a photovoltaic thermal cogeneration system. They used nanofluids for both cooling and heating in the system and introduced a new thermal conductivity model. They numerically investigated the effect of various parameters on the efficiency that reached as high as 70% for the nanofluid-based systems. Table 1 summarizes and compares various methods used for cooling down the photovoltaic thermal units introduced in the literature.

In this study, a combined experimental and numerical research is performed to investigate the performance of a PVT nanofluid-based collector system. Four different metal-oxides/water nanofluids are investigated in a PVT sheet-and-tube collector system. The considered nanoparticles include: Aluminum-oxide (Al_2O_3), Titanium-oxide (TiO_2) and Zinc-oxide (ZnO) all dispersed in deionized water as base fluid, with 0.2% by weight (wt%). To investigate the reliability of the measurements, an uncertainty analysis is performed for the experimental data. The electrical efficiency for the PVT system is calculated based on the measured temperature of the photovoltaic surface and the fluid outlet. For the numerical part, the energy equation for the whole system including the various layers of the PV module, absorber plate and fluid flow are solved using an in-house program. The *t-statistic* indicator is also used to verify that the results of the numerical model are statistically significant. To validate the simulations, the fluid outlet temperature and electrical efficiency are calculated from the numerical model and compared with those of the

Table 1
A summary of various methods used for cooling down the photovoltaic thermal units.

System type	Method of analysis	Characteristics
Hybrid photovoltaic/thermal water-heating system with natural circulation [2]	Experimental and numerical	Energy saving up to 65% Daily electrical efficiency: 10.15% Daily thermal efficiency exceeds 45% Total efficiency above 52%
Building-integrated photovoltaic thermal (BIPVT) water based collector [5]	Experimental and numerical	Electrical, thermal and combined efficiencies of the PVT (c-Si) were 11.6%, 51% and 63%, respectively.
High concentration PVT system [6]	Experimental and numerical	Thermal efficiency: numerically: 52%, experimentally: 48% Overall efficiency can exceed 70%.
Concentration PVT co-generation system using nanofluids for cooling and heating [7]	Numerical	Electrical efficiency: 11% Thermal efficiency: 59%

measurements. Next, from the various metal-oxides/water nanofluids considered in this study, a nanofluid with a better performance in terms of the electrical efficiency, surface temperature and fluid outlet temperature is selected. The numerical model is then used to examine the effects of various weight fractions of the selected nanofluid on the PVT performance.

2. Experimental setup

A view of the experimental setup is shown in Fig. 1. The experimental setup consists of a 40 W, mono-crystalline silicon, photovoltaic module (Suntech Co., China) equipped with a sheet-and-tube collector (called PVT for the rest of the paper). Mono-crystalline silicon photovoltaic modules are extensively used as typical PV modules with high electrical efficiency and low thermal resistance losses [23]. K-type sensors with a data logger (Testo – 177-T4, UK) are used for measuring and saving the temperature of the fluid at the inlet and outlet of the collector and that of the photovoltaic panel surface (PV). By using the data logger, temperature changes can be tracked in short step times (under 5 s) during the experimental period. The total incident irradiation is measured by a solar power meter (TES-1333, Taiwan) mounted parallel to the photovoltaic surface. A rotary flow meter (20–60 l/h) is used for measuring and fixing the flow rate at a constant value. The working fluid in all experiments has a constant mass flow rate of 30 kg/h. The working fluids considered in the experiments are pure water, aluminum-oxide/water, titanium-oxide/water and zinc-oxide/water nanofluids. All nano-oxides particles are dispersed in deionized water with 0.2 wt% by a high-speed stirrer and a proper surfactant [24] (nanoparticles properties can be seen in Table 2). The mixture is then stabilized under a continuous sonication using an ultrasonic vibrator for about 2 h (Wisd DH.WUC.D10H, Korea). The ultrasonic process time is divided into six-time periods of 20 min (with a total time of 2 h) at a set constant temperature of 60 °C. To examine the nanofluids stability, the density of the nanofluid at various points and times during the course of the experiment is measured. Although a slight sedimentation of nanoparticles was observed after 2 days, for the duration of each experiment (6 h) no significant changes in the density were observed. The daily measured data was collected from 9:30 a.m. to 3:30 p.m. on selected days in August and September at the Ferdowsi University of Mashhad, Mashhad, Iran (Latitude: 36° and Longitude: 59°). The performance of a PVT depends on solar irradiation. Based on the location (Mashhad, Iran) and the weather conditions, the optimum solar irradiation for thermal collector operation is selected from 9:30 a.m. till 15:30 p.m. (six hours for each day). It should be noted that although a PVT system can be used in other times during the day, the pumping power required to circulate the working fluid will not be compensated by the output of the PVT system; i.e., the net power output of the system will be negligible.

Sudden changes in weather conditions during a day, especially the solar irradiation due to clouds and ambient temperature can affect the result of the PVT system. To have more reliable results and less uncertainty, experiments are carried out over the month of August and September (stable weather condition, ambient temperature and solar irradiation).

Table 2
Nanoparticles properties.

Nanoparticle	Particle size (nm)	Density (kg/m^3)	Heat capacity (J/kg K)	Thermal conductivity (W/m K)
Al_2O_3	20	3970	765	40
TiO_2	10–30	4250	686	8.9
ZnO	10–25	5600	495	13

Fig. 1. A view of the experimental setup at the Ferdowsi University of Mashhad.

3. Numerical model

The mathematical model used to simulate the PVT system is based on the following assumptions:

- the Ohmic losses of the solar cells are neglected;
- the temperature of the fluid in the collector only varies in axial direction;
- the sky is assumed to be a black body with a temperature of T_{sky}; and
- the fluid flow in the tubes is assumed to be uniform.

It should be noted that these assumptions do not affect the results considerably. The Ohmic losses compared to the electrical output are negligible. Due to the small diameter of the copper pipe, the heat transfer in the fluid flow can be assumed lumped in the radial direction. Assuming a uniform fluid flow in the pipe is a usual assumption when studying the convection heat transfer in a pipe.

A schematic diagram of heat transfers in a cross-section of a selected control volume is shown in Fig. 2. The control volume includes the PV and collector components.

The energy balance equations for the system can be written in details as follows.

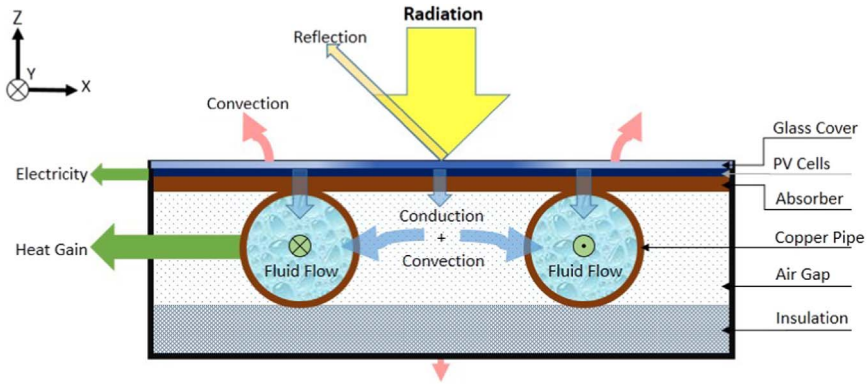

Fig. 2. A schematic diagram of heat transfer mechanisms in a cross-section of a selected control volume.

3.1. Glass cover

$$\rho_g \delta_g C_g \frac{dT_g}{dt} = \alpha_g G + h_{rad,g\to env}(T_{sky} - T_g) + h_w(T_{amb} - T_g) + h_{\mathrm{cond},g\to pv}(T_{pv} - T_g) \quad (1)$$

where the left hand side of the equation refers to the temporal energy changes in the glass cover. The first item of the right hand side is the received irradiation by the glass cover; the second item is the radiative heat transfer between the glass cover and the surroundings; the third item is the convective heat transfer between the glass cover and the outside environment; and the forth item is the conductive heat transfer from the photovoltaic cells to the glass cover. $h_{\mathrm{cond},g\to pv}$ is the equivalent conduction heat transfer coefficient. A similar procedure is established to obtain the rest of equations as follows.

3.2. Photovoltaic panel

$$\rho_{pv}\delta_{pv}C_{pv}\frac{dT_{pv}}{dt} = \alpha_{pv}\tau_g G - E_{elec} + h_{cond,pv\to g}(T_g - T_{pv}) + h_{cond,pv\to abs}(T_{abs} - T_{pv}) \quad (2)$$

In Eq. (2), τ_g is the transmittance coefficient of the glass cover.

3.3. Absorber plate

$$\rho_{abs}\delta_{abs}C_{abs}\frac{dT_{abs}}{dt} = h_{cond,pv\to pab}(T_{abs} - T_{pv}) + f_{abs,tube}\,h_{cond,abs\to tube}(T_{tube} - T_{abs}) + f_{abs,ins}\,h_{cond,abs\to ins}(T_{ins} - T_{abs}) \quad (3)$$

where, $f_{abs,tube}$ is defined as the contact factor of the absorber and the tube. In the numerical solution, this value is one (in the contact parts) or zero (in noncontact parts). A similar factor can be defined between the absorber and insulation as $f_{abs,ins}$.

3.4. Tubes

$$\rho_{tube}\delta_{tube}PdyC_{tube}\frac{\partial T_{tube}}{dt} = A_{abs,tube}\,h_{cond,\mathrm{abs}\to tu}(T_{tube} - T_{abs}) + h_{conv,tube\to f}Pdy(T_f - T_{tube}) + A_{ins,tube}\,h_{cond,tube\to ins}(T_{ins} - T_{tube}) \quad (4)$$

where P refers to the periphery of the tube.

3.5. Working fluid

$$\rho_f A_f dyC_f\frac{\partial T_f}{\partial t} = h_{conv,tube\to f}Pdy(T_{tube} - T_f) \quad (5)$$

3.6. Insulation

$$\rho_{ins}\delta_{ins}C_{ins}\frac{dT_{ins}}{dt} = h_{cond,ins\to tube}f_{tube,ins}(T_{tube} - T_{ins}) + f_{abs,ins}\,h_{cond,abs\to ins}(T_{abs} - T_{ins}) + h_w(T_{amb} - T_{ins}) \quad (6)$$

3.7. Heat transfer coefficients

The heat transfer coefficients used in the above equations are defined as follows. The irradiation heat transfer coefficient between the PV module and the sky is obtained as [25]:

$$h_{rad,g\to env} = \varepsilon_g\sigma(T_g^2 + T_{sky}^2)(T_g + T_{sky}) \quad (7)$$

where the temperature of the sky, T_{sky}, is calculated by the following empirical equation [26]:

$$T_{sky} = 0.0552{*}T_{amb}^{1.5} \quad (8)$$

The convective heat transfer coefficient due to the wind is described as [27]:

$$h_w = 5.7 + 3.8V_w \text{ if } V_w{<}5\frac{m}{s}$$
$$h_w = 6.47 + V_w^{0.78} \text{ if } V_w{>}5\frac{m}{s} \quad (9)$$

The convective heat transfer coefficient between the fluid and the tube $h_{conv,tube\to f}$, can be expressed as [28]:

$$\mathrm{Re} < 2300 \Rightarrow Nu = 4.364$$
$$\mathrm{Re} > 2300 \Rightarrow Nu = 0.023\,\mathrm{Re}^{0.8}\,\mathrm{Pr}^{0.4} \quad (10)$$

In Eq. (10), the Prandtl number can be calculated by:

$$\mathrm{Pr} = \frac{\mu_f C_{p,f}}{k_f} \quad (11)$$

The equivalent conduction heat transfer coefficient between two neighboring layers m and n can be expressed as [29]:

$$h_{cond,m\to n} = \frac{1}{\frac{\delta m}{k_m} + \frac{\delta n}{k_n}} \tag{12}$$

The specific heat capacity and density of the nanofluid can be calculated using the following equation introduced by Xuan and Roetzel [30]:

$$C_{p,nf} = C_{p,np}(\phi) + C_{p,bf}(1-\phi) \tag{13}$$

$$\rho_{p,nf} = \rho_{p,np}(\phi) + \rho_{p,bf}(1-\phi) \tag{14}$$

The thermal conductivity of the nanofluid can be calculated using the Hamilton and Crosser model [31]:

$$k_{nf} = \frac{(k_{np} + 2k_{bf}) + 2\varphi(k_{np} - k_{bf})]}{[(k_{np} + 2k_{bf}) - \varphi(k_{np} - k_{bf})]} \tag{15}$$

In above equations, the subscripts *bf* and *p* indicate the base fluid and particle, respectively.

In this study, the Corcione model [32] is used to calculate the viscosity of nanofluids:

$$\mu_{nf} = \frac{\mu_f}{1 - 34.87\left(\frac{d_{np}}{d_{bf}}\right)^{-0.3}\varphi^{1.03}} \tag{16}$$

where d_{np} and d_{bp} indicate the diameter of the nanoparticles and the base fluid molecular diameter, respectively.

The electrical efficiency can be calculated as the net output electrical power to the input energy of the sun [9]:

$$\eta_{elec} = \frac{\dot{E}_{elec}}{\dot{E}_{in}} = \frac{V_{oc} \times I_{sc} \times FF}{\dot{G}_{effective}} \tag{17}$$

where V_{oc} is the open circuit voltage, I_{sc} is the short circuit current and FF indicates the Filled factor [9].

3.8. Numerical procedure

The energy balance equations (Eqs. (1)–(6)) are solved using a 2D transient model based on a control volume method and an implicit scheme. The entire computational domain is discretized using a uniform structured 120*100 mesh. This grid value is chosen based on the mesh independency analyses for a 64*54 cm PVT dimension. A flowchart diagram of the numerical procedure is presented in Fig. 3. The system initial properties include: geometric parameters of the entire system such as the tube diameter; and the thickness of the glass cover, PV cells, and absorber; as well as thermo-physical properties such as the glass cover transitivity, absorption coefficient, and working fluid properties. Other required inputs include: solar irradiation, ambient temperature, working fluid mass flow rate, wind velocity, and fluid inlet temperature to the collector; these values are those measured in the experiments. At the beginning of the simulation, the initial temperature of the PV, absorber plate, tube and insulation is the ambient temperature. The initial temperature of the entire working fluid is assumed to be equal to that of its inlet to the collector. Since the energy equations are solved implicitly, several iterations are required at each time step. The iterations are continued until the differences of the calculated temperature between two sequential time steps, for all computational nodes, is less than a tiny value (e.g. 10^{-6}). The computations are continued until a desired time.

3.9. Uncertainty analysis and model verification

In order to determine the reliability of experiments, an uncertainty analysis is performed for the measured parameters and

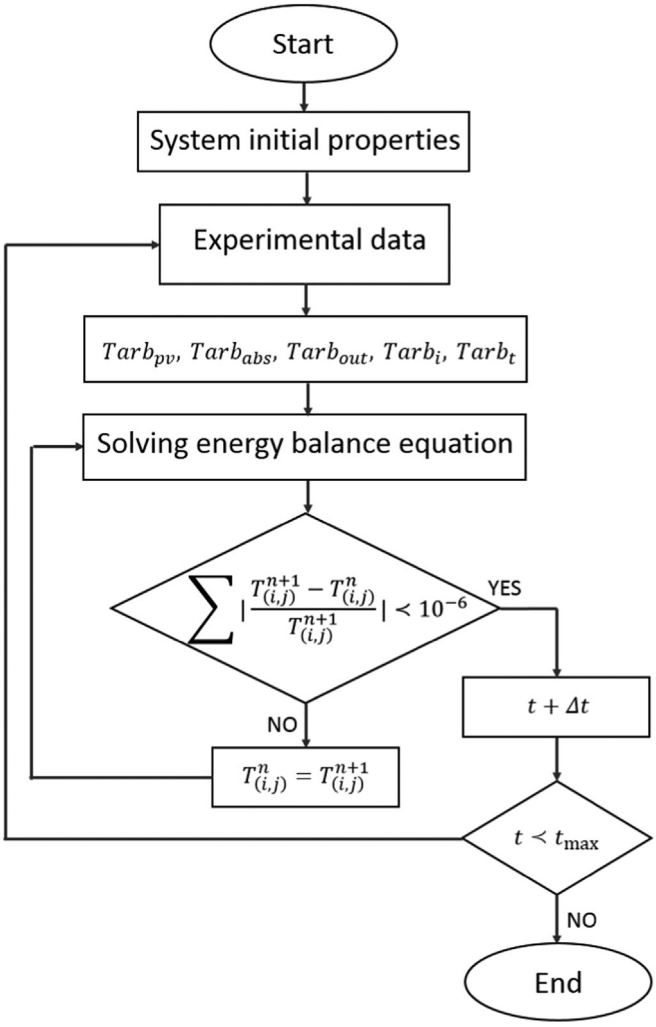

Fig. 3. A flowchart diagram of the numerical procedure.

electrical efficiency [9]. If R is a function of 'n' independent linear parameters as $R = R(v_1, v_2, v_3, \ldots v_n)$, the uncertainty of function R may be calculated as:

$$\delta R = \sqrt{\left(\frac{\partial R}{\partial v_1}\delta v_1\right)^2 + \left(\frac{\partial R}{\partial v_2}\delta v_2\right)^2 + \ldots + \left(\frac{\partial R}{\partial v_n}\delta v_n\right)^2} \tag{18}$$

where δR is the uncertainty of function R, δv_i the uncertainty of parameter v_i, and $\partial R/\partial v_i$ is the partial derivative of R with respect to parameter v_i. Also, the *t-statistic* (*t-test*) model is used to determine the reliability of the numerical model for each calculated parameter compared to that of the experiment. This statistical indicator permits the numerical simulations to be compared with measurements, and at the same time can specify whether or not the model predictions are statistically significant at a specific confidence level [33]. In the *t*-test model, both the root mean-square error (RMSE) and mean bias error (MBE) are considered. If n indicates the number of data pairs (numerical/experimental results), the RMSE and MBE are given by:

$$\text{RMSE} = \left(\frac{1}{n}\sum_{i=1}^{n} d_i^2\right)^{1/2} \tag{19}$$

$$MBE = \frac{1}{n}\sum_{i=1}^{n} d_i \tag{20}$$

where d_i is the point to point difference between of the i^{th} numerical result and the measured value. In the present study, the number of data is considered to be 13 points in each experimental period.

Based on the above equations, the *t-statistic* is given as [33]:

$$t = \left(\frac{(n-1)\mathrm{MBE}^2}{\mathrm{RMSE}^2 - \mathrm{MBE}^2}\right)^{1/2} \tag{21}$$

Before each analysis, a normality test for each set of data is performed based on the Kolmogorov-Smirnov model.

4. Results and discussion

The uncertainty of experiments is found to be less than 5% for all cases considered in this paper based on Eq. (18). More details with this regard can be seen elsewhere [9].

As can be seen in Table 3, the hypothesis of normality is confirmed based on the asymptotic significance (2-tailed) level of more than 0.05 for all cases.

Since the P-values are more than 0.05, all data sets are normal; therefore, the *t-test*, which is a parametric test, can be used. To determine whether the numerical simulations are statistically significant, the critical t value is obtained $t_{critical}=3.055$ from the standard statistical tables for a P-value of 0.01 and 12 degrees of freedom. The smaller the value of t (smaller than the critical t), the better is the model performance [33]. The t-test results are summarized in Table 4.

As seen in the table, the numerical model works well for most cases with a good precision for both temperature and electrical efficiency especially for the ZnO/water and TiO_2/water nanofluids. The small discrepancies between simulations and measurements can be attributed to the experimental adverse factors, such as air humidity, wind velocity, etc.

The daily measured data was collected from 9:30 a.m. to 3:30 p.m. on selected days in August and September at the Ferdowsi University of Mashhad, Mashhad, Iran (Latitude: 36° and Longitude: 59°). The average daily summaries of the measured weather data during the experiments are shown in Fig. 4. Based on this data, the average total incident irradiation and the average ambient temperature are determined to be nearly 917 W/m^2 and 33.4 °C, respectively. Based on the experimental data and the Re number for all working fluids is calculated under 2300 which shows a laminar regime.

4.1. Surface temperature

The experimental and numerical results for the variation of the PVT surface temperature, and also the experimental results for the variation of the PV surface temperature are shown in Fig. 5a–d. As can be seen, the calculated temperatures are in good agreements with those of the experiments for all cases considered. For the deionized water, the difference between the calculated and measured surface temperatures is maximum, which is less than 2.4% (Fig. 5a). By using a thermal collector, a considerable decrease in the surface temperature can be achieved during the day compared to that of a PV system. The difference in the surface temperature of the PV and PVT systems is higher at the peak of the irradiation (around 13:00 local time). A close inspection of these results shows that the average surface temperature reduction of the PVT system (measured values) compared to that of the PV for the duration of the experiments (9:30 a.m. till 15:30) is 11.0, 11.48, 11.85 and 11.03 °C, for deionized water, the TiO_2/water, ZnO/water and Al_2O_3/water, respectively. This result indicates the best thermal performance for the ZnO/water nanofluid compared to deionized water and other nanofluids.

Table 3
Significance values of the Kolmogorov-Smirnov model (normality test), P-values.

Parameter		Water	TiO_2/water	ZnO/water	AL_2O_3/water
Collector outlet temperature	Experimental	0.49	0.39	0.29	0.29
	Numerical	0.31	0.32	0.36	0.35
Surface temperature	Experimental	0.71	0.59	0.60	0.70
	Numerical	0.76	0.41	0.59	0.48
Electrical efficiency	Experimental	0.83	0.74	0.48	0.55
	Numerical	0.77	0.43	0.69	0.48

Table 4
The *t-statistic* model results.

Parameter	Water	TiO_2/water	ZnO/water	AL_2O_3/water	Critical t
Collector outlet temperature	5.10	0.38	4.11	2.37	3.055
Surface temperature	4.39	3.81	1.93	3.11	3.055
Electrical efficiency	2.00	3.00	3.01	7.48	3.055

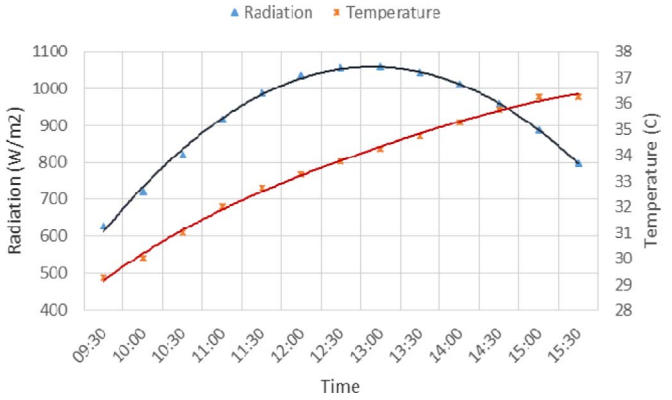

Fig. 4. Average daily variation of the total irradiation and ambient temperature during the test period.

4.2. Electrical efficiency

Experimental and numerical results of the electrical efficiency for the same cases as of Fig. 5 are shown in Fig. 6a–d. By using a solar thermal collector, an increase of the electrical efficiency is observed for all cases considered. The electrical efficiency obtained from the numerical simulations is close to that of the experiments; the average difference between the two values is less than 2.2% in all cases considered. As seen in Fig. 6a–d, the average increase in the electrical efficiency of the PVT system compared to that of the PV is around 5.48%, 6.54%, 6.46% and 6.36% for deionized water, the TiO_2/water, ZnO/water and Al2O3/water, respectively. Therefore, it can be concluded that although for the ZnO/water nanofluid, a more reduction of the average surface temperature is observed, for the TiO_2/water nanofluid, the average electrical efficiency is higher. This is because of a more uniform distribution in the surface temperature reduction for the TiO_2/water nanofluid compared to that of the ZnO/water (Fig. 5b and c).

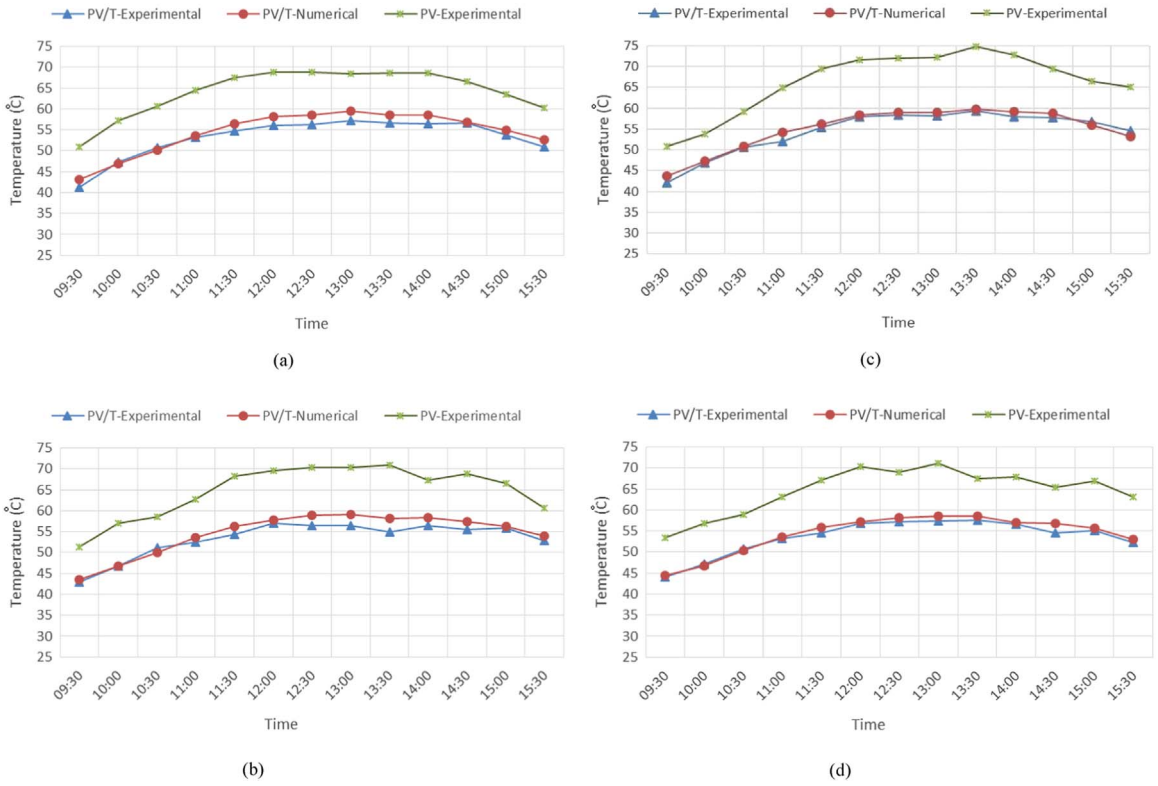

Fig. 5. Measured and calculated surface temperatures of the PVT system in comparison with measured values of the PV system for the case of (a) deionized water, (b) TiO_2/water nanofluid, (c) ZnO/water nanofluid and (d) Al_2O_3/water nanofluid.

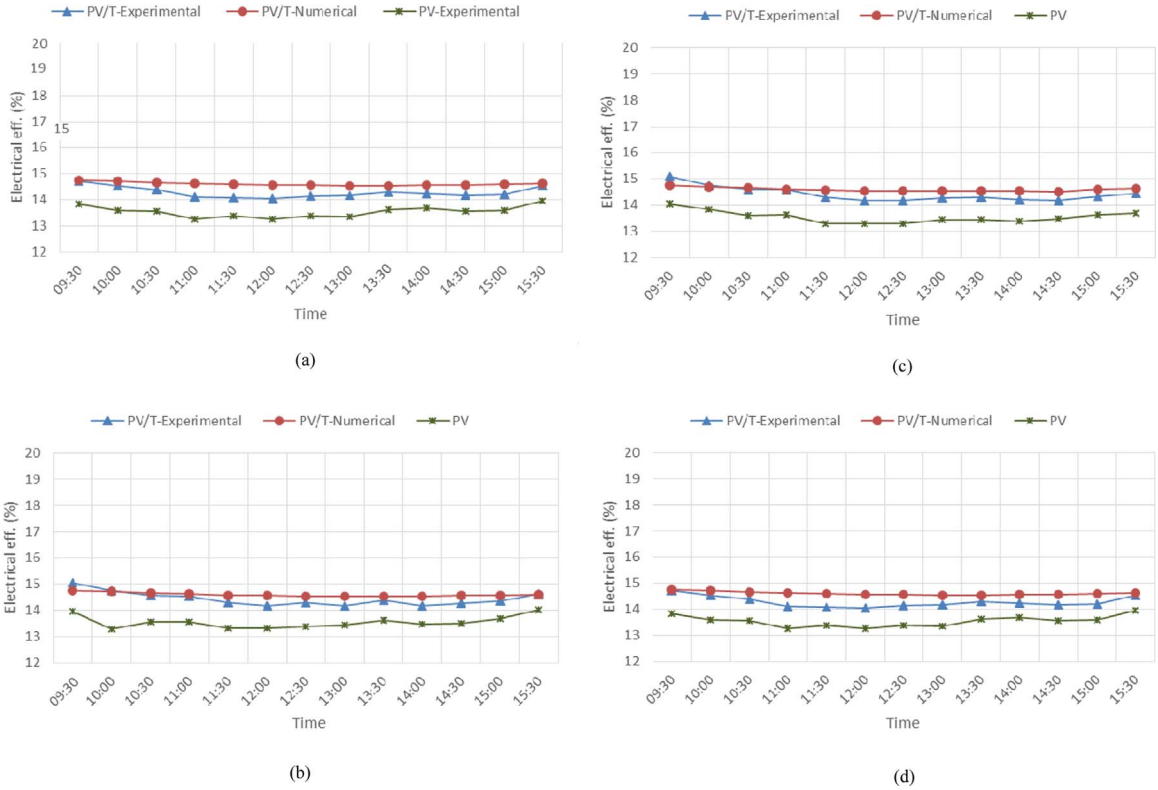

Fig. 6. Measured and calculated electrical efficiency of the PVT system in comparison with measured values of the PV system for the case of (a) deionized water, (b) TiO_2/water nanofluid, (c) ZnO/water nanofluid and (d) Al_2O_3/water nanofluid.

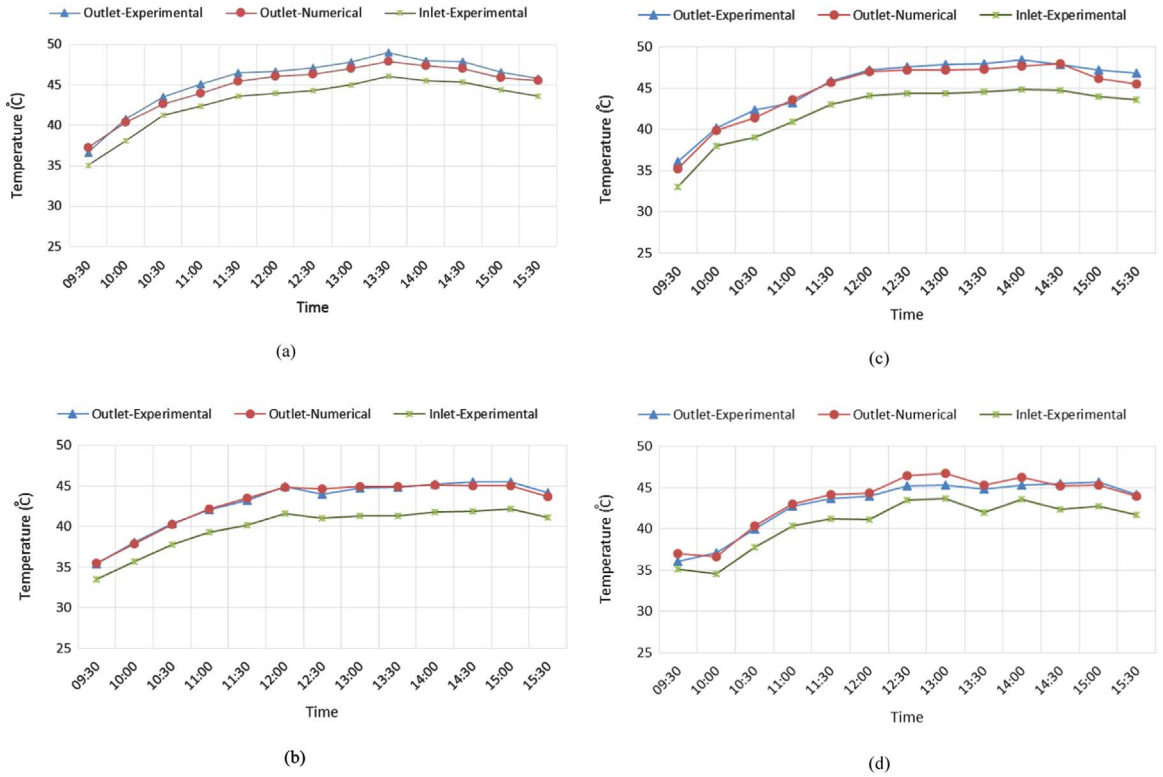

Fig. 7. Measured and calculated fluid outlet temperature of the PVT system in comparison with measured values of the PV system for the case of (a) deionized water, (b) TiO_2/water nanofluid, (c) ZnO/water nanofluid and (d) Al_2O_3/water nanofluid.

4.3. Outlet collector temperature

The calculated and measured values of the collector outlet temperatures are displayed in Fig. 7a–d; the average difference between the two results is less than 1.5% for all cases. The difference between the measured fluid inlet temperature and that of the collector outlet are 2.31, 3.02, 3.11 and 2.50 °C, for the case of deionized water, the TiO_2/water, ZnO/water and Al_2O_3/water nanofluids, respectively. This temperature difference is directly related to the thermal efficiency of the collector. A close inspection of the results shown in Fig. 7a–d, reveals that the average temperature difference between the collector inlet and outlet is maximum for the ZnO/water and minimum for the Al_2O_3/water nanofluids. This, in turn, leads to the best thermal performance for the ZnO/water nanofluid and the worst for the Al_2O_3/water. As the results of Fig. 7a–d show, the fluid inlet temperature of the collector increases in the duration of the experiments due to the closed circulation system used for the working fluid.

4.4. System cost analysis

Bhattarai et al. [34], performed a comparative study of photovoltaic and thermal solar systems water based collector. They concluded that the cost payback period of the PVT system is lower than that of the PV module and higher than the conventional solar thermal collector. Faizal et al. [35] found that using nanofluids in solar collectors results in more energy savings and a smaller size system with less emission of CO_2. The experimental studies in the literature on the economic aspects of using nanofluids in the PVT systems are rare and the cost can vary by local energy cost and government subsidies. System size reduction analysis can be a helpful method from the cost viewpoint.

Average daily electrical and thermal output are shown in Fig. 8a for all experimented cases.

Based on the energy output of each system, a cost analysis is applied for all systems based on 1 kW overall energy output generation (thermal and electrical). In order to generate 1 kW electrical power, 46 PV units are required if each PV unit produces 40 W. From the energy viewpoint, by using pure water, the PVT/TiO_2, PVT/ZnO and PVT/Al_2O_3, the size reduction of the PVT system compared to that of the PV is 21%, 32%, 33% and 24%, respectively (see Fig. 8).

4.5. Effects of nanoparticles mass fraction

Based on the experimental results of either the fluid outlet temperature (Fig. 6a–d) or the electrical efficiency (Fig. 5a–d), the TiO_2/water and ZnO/water nanofluids show a better performance in the PVT system. For the ZnO/water nanofluid, however, the thermal performance is preferred over the TiO_2/water. Hence, the ZnO/water may be considered to be the best nanofluid amongst the investigated working fluids in this study. Next, the numerical model is used to examine the effects of various weight fractions of this nanofluid on the electrical efficiency, surface temperature and fluid outlet temperature. The results are displayed in Fig. 9a and b and Fig. 10, for nanoparticle mass fractions ranged from 0.05 to 10 wt%. Based on these results, increasing the nanoparticles mass fraction from 0.05 to 10% reduces the surface temperature by nearly 2%. Therefore, the increase of nanoparticle mass fraction slightly reduces the surface temperature (Fig. 9a) which, in turn, translates into a slight increase of the electrical efficiency (Fig. 9b). The main effect of the nanoparticle mass fraction is on the thermal performance of the system. By increasing the mass fraction of nanoparticles from 0.05 to 10 wt%, the thermal performance of the system increases by four times (see Fig. 10).

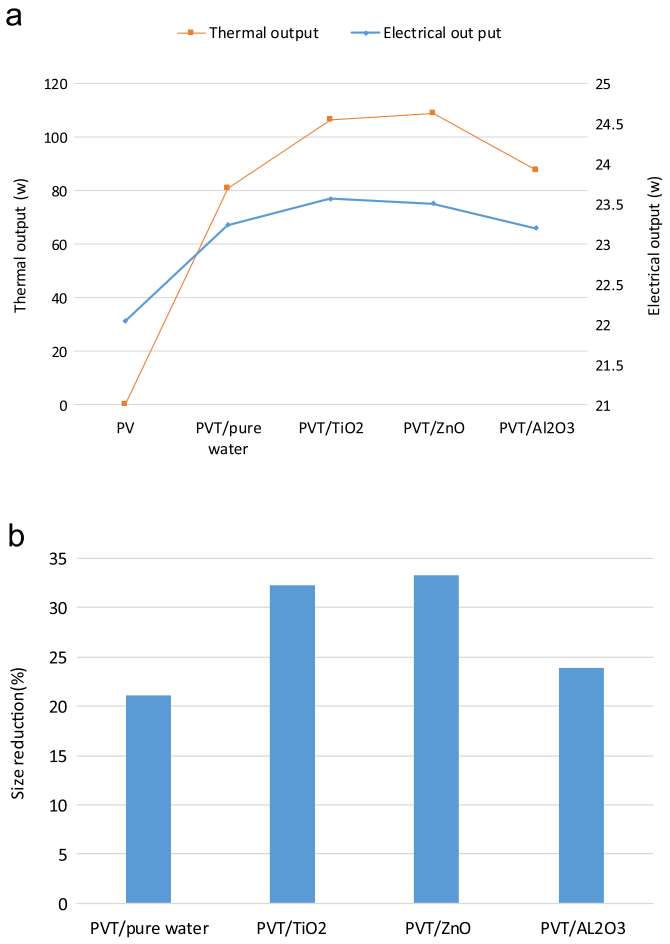

Fig. 8. (a) Average daily electrical and thermal output of the PV and PVT systems. (b) System size reduction based on 1 kW overall energy output generation (thermal and electrical) for various cooling systems compared to that of a conventional PV module.

5. Conclusions

In this study, a combined experimental/numerical approach was used to investigate the cooling of a PVT system by metal-oxides/water nanofluids. The experimental results of various nanofluids were compared with each other and also with those of a PV system as a conventional photovoltaic unit. The measured values for the surface temperature, the electrical efficiency, and the collector outlet temperature were used to investigate the various aspects of the PVT system performance and verify the calculated values obtained from the numerical model. The working fluids considered in this study were deionized water, the TiO_2/water, ZnO/water, and Al_2O_3/water. Numerical results agreed well with those of the experiments for all cases considered. Both experimental and numerical results revealed that the most significant effect of using metal-oxides/water nanofluids is on the thermal performance of the system. Based on this analysis, the ZnO/water nanofluid showed a better thermal performance compared to other working fluids. The numerical model was then applied to study the effects of the ZnO nanoparticle mass fraction on the PVT performance. The results showed that while the thermal performance of the PVT system is highly dependent on the mass fraction of the nanoparticles, the electrical efficiency is slightly changed when the mass fraction is varied. Increasing the mass fraction of nanoparticles from 0.05 to 10 wt% increased the thermal performance of the system by nearly four times. The surface temperature, however, was reduced by only 2% which, in turn, resulted in a slight increase of the electrical efficiency by 0.02%. As a result, apart from the preparation cost and nanofluid stabilization difficulties, when the net thermal energy obtained from a PVT system is of interest, using metal-oxides/water nanofluids with a high mass fraction will considerably improve the thermal performance of the system.

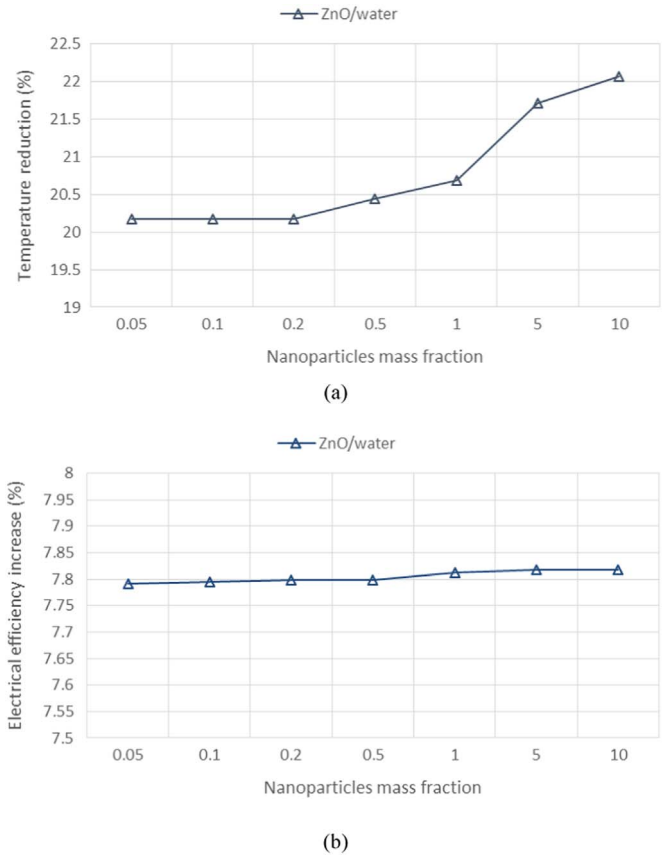

Fig. 9. The effect of the ZnO nanoparticle mass fraction on (a) average surface temperature reduction and (b) average relative electrical efficiency increase, of the PVT system when compared to the measured values of the PV system.

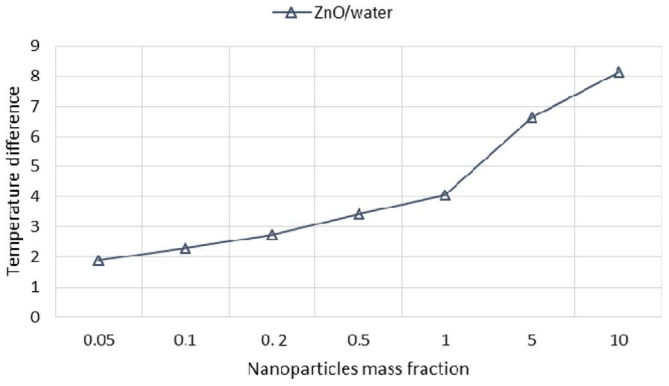

Fig. 10. The effect of the ZnO nanoparticle mass fraction on the average temperature difference of the nanofluid between the inlet and outlet of the collector for different mass fractions of nanoparticles.

References

[1] A. Ibrahim, M.Y. Othman, M.H. Ruslan, S. Mat, K. Sopian, Recent advances in flat plate photovoltaic/thermal (PV/T) solar collectors, Renew. Sustain. Energy

Rev. 15 (2011) 352–365.
[2] J. Ji, J.P. Lu, T.T. Chow, W. He, G. Pei, A sensitivity study of a hybrid photovoltaic/thermal water-heating system, Nat. Circ. Appl. Energy 84 (2007) 222–237.
[3] F. Shan, F. Tang, L. Cao, G. Fang, Comparative simulation analyses on dynamic performances of photovoltaic/thermal solar collectors with different configurations, Energy Convers. Manag. 87 (2014) 778–786.
[4] B.M. Ziapour, M. Palideh, M. Baygan, Performance comparison of four passive types of photovoltaic–thermal systems, Energy Convers. Manag. 88 (2014) 732–738.
[5] R. Daghigh, A. Ibrahim, G.L. Jin, M.H. Ruslan, K. Sopian, Predicting the performance of amorphous and crystalline silicon based photovoltaic solar thermal collectors, Energy Convers. Manag. 52 (3) (2011) 1741–1747.
[6] H. Chen, J. Ji, Y. Wang, W. Sun, G. Pei, Z. Yu, Thermal analysis of a high concentration photovoltaic/thermal system, Sol. Energy 107 (2014) 372–379.
[7] Z. Xu, C. Kleinstreuer, Concentration photovoltaic–thermal energy co-generation system using nanofluids for cooling and heating, Energy Convers. Manag. 87 (2014) 504–512.
[8] M.N. Abu-Bakara, M. Othman, M. Hj Dina, N.A. Manaf, H. Jarimi, Design concept and mathematical model of a bi-fluid photovoltaic/thermal (PV/T) solar collector, Renew. Energy 67 (2014) 153–164.
[9] M. Sardarabadi, M. Passandideh-Fard, S. Zeinali Heris, Experimental investigation of the effects of silica/water nanofluid on PV/T (photovoltaic thermal units), Energy 66 (2014) 264–272.
[10] A. Ibrahim, M.Y. Othman, M.H. Ruslan, S. Mat, K. Sopian, Recent advances in flat plate photovoltaic/thermal (PV/T) solar collectors, Renew. Sustain. Energy Rev. 15 (2011) 352–365.
[11] J.F. Cerón, J. Pérez-García, J.P. Solano, A. García, R. Herrero-Martín, A coupled numerical model for tube-on-sheet flat-plate solar liquid collectors. Analysis and validation of the heat transfer mechanisms, Appl. Energy 140 (2015) 275–287.
[12] X. Zhang, X. Zhao, J. Shen, J. Xu, X. Yu, Dynamic performance of a novel solar photovoltaic/loop-heat-pipe heat pump system, Appl. Energy 114 (2014) 335–352.
[13] K. Khanafer, K. Vafai, A critical synthesis of thermo-physical characteristics of nanofluids, Int. J. Heat Mass Transf. 54 (2011) 4410–4428.
[14] J. Koo, C. Kleinstreuter, Impact analysis of nanoparticle motion mechanisms on the thermal conductivity of nanofluids, Int. Commun. Heat Mass Transf. 32 (2005) 1111–1118.
[15] E.E. Michaelides, Z.-G. Feng, Heat transfer from a rigid sphere in a non-uniform flow and temperature field, Int. J. Heat Mass Transf. 37 (1994) 2069–2076.
[16] D. Lee, J.W. Kim, B.G. Kim, A new parameter to control heat transport in nanofluids: surface charge state of the particle in suspension, J. Phys. Chem. B 110 (2006) 4323–4328.
[17] X. Wu, H. Wu, P. Cheng, Pressure drop and heat transfer of Al_2O_3-H_2O nanofluids through silicon micro-channels, J. Micromech. Micro-Eng. 19 (2009) 105020.
[18] P.K. Nagarajan, J. Subramani, S. Suyambazhahan, R. Sathyamurthy, Nanofluids for solar collector applications: a review, Energy Procedia 61 (2014) 2416–2434.
[19] K.S. Suganthi, V.L. Vinodhan, K.S. Rajan, Heat transfer performance and transport properties of ZnO–ethylene glycol and ZnO–ethylene glycol–water nanofluid coolants, Appl. Energy 135 (2014) 548–559.
[20] S. Bhattarai, J.H. Oh, S.H. Euh, G.K. Kafle, D.H. Kim, Simulation and model validation of sheet and tube type photovoltaic thermal solar system and conventional solar collecting system in transient states, Sol. Energy Mater. Sol. Cells 103 (2012) 184–193.
[21] W. He, J. Zhou, C. Chen, J. Ji, Experimental study and performance analysis of a thermoelectric cooling and heating system driven by a photovoltaic/thermal system in summer and winter operation modes, Energy Convers. Manag. 84 (2014) 41–49.
[22] H. Dehra, A two dimensional thermal network model for a photovoltaic solar wall, Sol. Energy 83 (2009) 1933–1942.
[23] V. Kanchan, G.N. Tiwari, Energy and exergy analysis of a building integrated semitransparent photovoltaic thermal (BISPVT) system, Appl. Energy 96 (2012) 409–416.
[24] Z. Haddad, C. Abid, H.F. Oztop, A. Mataoui, A review on how researchers prepare their nanofluids, Int. J. Therm. Sci. 76 (2014) 168–189.
[25] O. Rejeb, H. Dhaou, A. Jemni, Parameters effect analysis of a photovoltaic thermal collector: case study for climatic conditions of Monastir, Tunisia, Energy Convers. Manag. 89 (2014) 409–419.
[26] S.L. Swinbank, Long-wave radiation from clear skies, Q. J. R. Meteorol. Soc. 89 (1963) 339.
[27] W.H. McAdams, Heat Transmission, 3rd ed., Mcgraw-Hill, New York, 1954.
[28] A. Bejan, Heat Transfer, Wiley, New York, 1993.
[29] J.A. Duffie, W.A. Beckman, Solar Engineering of Thermal Processes, John Wiley & Sons Inc., New York, 1990.
[30] Y. Xuan, W. Roetzel, Conceptions for heat transfer correlation of nanofluids, Int. J. Heat Mass Transf. 43 (2000) 3701–3707.
[31] R.L. Hamilton, O.K. Crosser, Thermal conductivity of heterogeneous two component systems, Ind. Eng. Chem. Fundam. 1 (1962) 187–191.
[32] M. Corcione, Empirical correlating equations for predicting the effective thermal conductivity and dynamic viscosity of nanofluids, Energy Convers. Manag. 52 (2011) 789–793.
[33] R.J. Stone, Improved statistical procedure for the evaluation of solar radiation estimation, Sol. Energy 51 (1993) 289–291.
[34] S. Bhattarai, G.K. Kafle, S.H. Euh, J.H. Oh, Comparative study of photovoltaic and thermal solar systems with different storage capacities: performance evaluation and economic analysis, Energy 61 (1993) 272–282.
[35] M. Faizal, R. Saidur, S. Mekhilef, M.A. Alim, Energy, economic and environmental analysis of metal oxides nanofluid for flat-plate solar collector, Energy Convers. Manag. 76 (2013) 162–168.